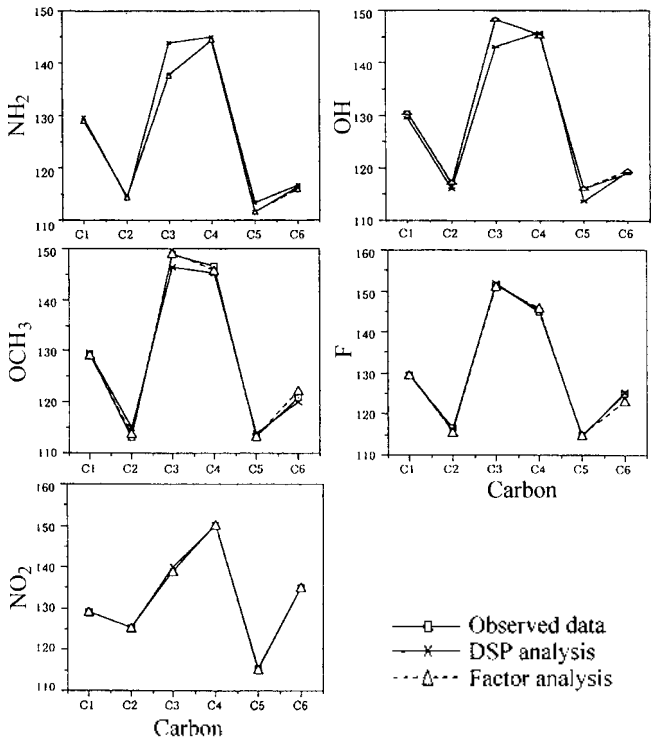

Figure 4. Plot of carbon-13 chemical shift calculated by DSP and factor analysis.

second factor, a_2, has no correlations with commonly used empirical parameters. Considering the values of communalities, this effect is dominated at ipso and meta carbons and it may be considered as an electric field effect or a steric effect. The third factor, a_3, has some correlations with substituent electronegativities[10,11] and shows the pattern which diminishes with increasing distance from the position of substitution. This behavior is very similar to that of inductive effect. ^{13}C chemical shifts reproduced by two methods are plotted in Figure 4 and compared with the observed data. It can be seen clearly that DSP analysis gives a over- and/or underestimated results at carbons 3 and 5 in the cases of NH_2, OH, and OCH_3. However, the results of three factor analysis are in full accord with the observed data. This implies that extra parameter should be needed to explain the ^{13}C chemical shifts of polysubstituted benzenes or that empirical parameters should be corrected in the case of polysubstituted benzenes.

References

1. Lee, S. G.; Choi, J.-K.; Park, N. S.; Hong, M. S.; Ha, D. C. *Bull. Korean Chem. Soc.* **1992**, *13*, 87.
2. Kalinowski, H. O.; Berger, S.; Braun, S. *Carbon-13 NMR Spectroscopy*; John Wiely & Sons: 1988.
3. Arunachalam, J.; Gangadharan, S. *Anal. Chim. Acta* **1984**, *157*, 245.
4. Kubista, M.; Sjoback, R.; Albinsson, B. *Anal. Chem.* **1993**, *65*, 994.
5. Zalewski, R. I.; Schneider, H. J.; Buchheit, V. *Mag. Res. Chem.* **1992**, *30*, 45.
6. Park, N. S.; Choi, J.-K.; Hong, M. S.; Kim, H. S.; Lee, J. C.; Choi, S. W.; Lee, B. Y.; Ha, D. C. Korea *J. Med. Chem.* **1993**, *3*, 142 and references cited therein.
7. *STATGRAPHICS* ver. 7, Manugistics Inc.: 2115 East Jefferson Street Rockville, MD 20852-4999 U.S.A.
8. Kessler, H.; Gehrke, M.; Greisinger, C. *Angew. Chem. Int. Ed. Engl.* **1988**, *27*, 490.
9. Hutton, H. M.; Kunz, K. R.; Bozek, J. D.; Blackburn, B. J. *Can. J. Chem.* **1987**, *65*, 1316 and references cited therein.
10. Inamoto, N.; Masuda, S. *Chem. Lett.* **1982**, *1003*, 1007.
11. Marriott, S.; Reynolds, W. F.; Taft, R. W.; Topsom, R. D. *J. Org. Chem.* **1984**, *49*, 959.

Zinc Oxide Nano-Cluster Formation in Zeolites

Hoo Bum Lee, Hyung Mi Lim, and Chong Soo Han*

Department of Chemistry, Chonnam National University, Kwangju 500-757, Korea
Received March 11, 1998

The quantum size effects in semiconductor clusters have been investigated in the hope of developing a novel type of opto-electronic devices.[1-3] It is possible to generate well-defined clusters in zeolite pores, which would provide fine tuning of electronic properties using large variety of zeolites with different cage sizes if the zeolite pores are successfully filled with semiconductor particles. The elemental clusters, such as Se and Te clusters,[3] and compound clusters, such as CdO_x, CdS, WO, GaP and CdSe clusters, are successfully embedded in zeolites.[4-6] The elemental clusters are synthesized by direct absorption from the vapor phase. The compound clusters are usually synthesized by ion-exchange in aqueous solution or deposition of MOCVD reagent, followed by subsequent treatments. For the case of ZnO, there are sparse reports on the formation and characterization of ZnO cluster in zeolite. The value of such clusters would be promising if taking advantage of the useful properties of ZnO-ZnO nano interface.[7,8] We report ZnO cluster formation in zeolite Y and zeolite A by oxidation of Zn loaded zeolite, which was synthesized by Zn vapor deposition.[9] Small shift of peaks and change of relative peak intensities in XRD spectra of the samples from those of zeolites prior to Zn vapor

deposition may indicate the ZnO cluster formation in the zeolite cage. The effect of Zn loading condition on the formation of ZnO clusters are discussed.

Experimental

Zeolite Na-Y was synthesized by mixing 13.5 g sodium aluminate (0.05 mole alumina and 0.07 mole Na_2O) and 10 g sodium hydroxide (0.25 mole) in 70 g of water with vigorous stirring, followed by addition of 100 g of 30% silica sol (0.5 mole SiO_2). It was aged for 24 h at room temperature and for 48 h at 95 °C. It was filtered, washed, and dried at 110 °C. Then the powder was ion exchanged with 0.1 M NH_4Cl, dried at 110 °C and calcined in thin bed condition at 450 °C for 5 h to obtain zeolite H-Y.

Zeolite Na-A was synthesized as the following procedure.[10] 13.5 g sodium aluminate and 25 g sodium hydroxide were dissolved in 300 mL of water and heated, and then 14.2 g sodium metasilicate was added. It was aged at 90 °C for 5 h until the suspension settles, which is filtered, washed with distilled water, and dried at 100 °C.

Synthesized zeolite H-Y and Zeolite Na-A were confirmed by X-ray diffraction (D MAX2400. Rigaku, Japan). Zeolite H-Y and Na-A were evacuated at ca. 10^{-5} Torr at 120 °C for 2 h and exposed to Zn vapor (ca. 0.2 Torr) for 3 h, 6 h, 9 h, and 12 h at 450 °C. The zeolite exposed to Zn vapor was oxidized in air at 450 °C for 2 h to form ZnO in the presence of zeolite. The effect of the exposure time of Zn vapor with zeolite on the formation of ZnO clusters in zeolite (ZnO/H-Y and ZnO/Z-A) was studied by X-ray diffraction, Ultraviolet-Visible Diffuse Reflectance (HITACH (U-3501), Japan), and elemental analysis by Inductively Coupled Plasma (ICP). The properties of ZnO in zeolite were compared with those of bulk ZnO.

Results and Discussion

In Figure 1, the XRD spectra of zeolite H-Y, ZnO/H-Y with different exposure time to Zn vapor, and that of bulk ZnO are compared. The XRD of zeolite H-Y in Figure 1-a was compared with the reference spectrum[11] to confirm the formation of zeolite H-Y. For the sample of H-Y after the exposure to Zn vapor for 6 h, characteristic XRD peaks of ZnO over 30 degree do not appear as shown in Figure 1-b. However, for the samples with longer exposure time (Figure 1-c and 1-d), XRD peaks corresponding to ZnO appear. The fact suggests a formation of ZnO in H-Y. The principal features of the XRD peaks are the same as those of H-Y in the 2θ range of 5-40 degree. This means that ZnO loaded zeolite maintains the same framework of H-Y. The small differences of 2θ in various samples (Table 1) indicate very slight changes of structures among those samples that might have caused by ZnO inclusion. There are differences in relative XRD peak intensities among zeolite H-Y and ZnO loaded zeolites, which could be another evidence of ZnO confinement in zeolite.[12]

UV-VIS DRS of zeolite H-Y, ZnO/H-Y with different exposure time to Zn vapor, and bulk ZnO are shown in Figure 2. Several peaks in the range of 280-330 nm are observed in every sample except zeolite H-Y. These peaks in that wavelength are very similar to those observed for Zn

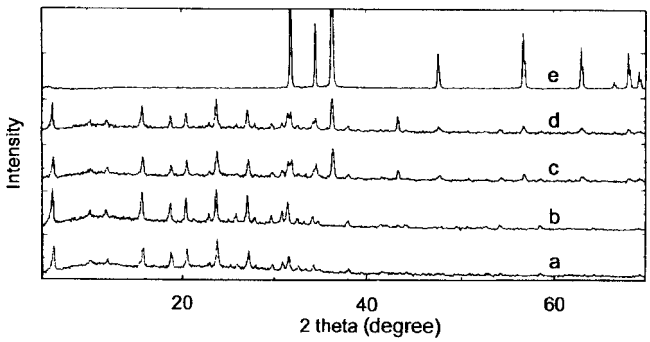

Figure 1. XRD spectra of (a) H-Y, Zeolite H-Y after the exposure to Zn vapor for (b) 6 h (c) 9 h (d) 12 h followed by oxidation in the air at 450 °C, and (e) bulk ZnO powder.

Table 1. Relative intensities of selected XRD peaks compared to the peak of $2\theta \cong 24°$ for (a) H-Y, Zeolite H-Y after the exposure to Zn vapor for (b) 6 h (c) 9 h (d) 12 h followed by oxidation in the air at 450 °C, and (e) bulk ZnO powder

a		b		c		d		e	
2θ	I/I_0	2θ	I/I_0	2θ	I/I_0	2θ	I/I_0	2θ	I/I_0
6.26	85	6.31	78	6.28	80	6.29	94		
10.24	46	10.23	39	10.23	26	10.21	41		
18.80	74	18.84	61	18.75	43	18.76	67		
23.68	100	23.75	100	23.73	100	23.74	100		
31.54	76	31.56	58	31.47	59	31.47	69		
				31.83	59	31.89	73	31.84	65
				34.42	50	34.51	58	34.50	43
				36.26	109	36.33	120	36.32	100
				47.60	23	47.58	19	47.62	26
				56.63	29	56.64	34	56.62	42

$(OH)_2$ and Zn^{2+} ion exchanged zeolite Y. The agreement suggests the peaks are originated from Zn^{2+} ion in similar environment. On the other hand, several peaks skewed to longer wavelength are growing in the range of 330-390 nm with longer exposure times. This suggests that the extent of ZnO formation increases with longer exposure time to Zn vapor. The onset of the peak indicates band gap energy and often used as a criterion of the nanocluster formation. The band gap energy of ZnO bulk is about 3.2 eV (390 nm). It

Table 2. Relative intensities of selected XRD peaks compared to the peak of $2\theta \cong 30°$ for (a) Na-A, Zeolite Na-A after the exposure to Zn vapor for (b) 3 h (c) 12 h followed by oxidation in the air at 450 °C, and (d) bulk ZnO powder

a		b		c		d	
2θ	I/I_0	2θ	I/I_0	2θ	I/I_0	2θ	I/I_0
10.20	47	10.19	89	10.21	53		
24.01	88	24.01	100	24.00	83		
27.15	83	27.13	92	27.14	93		
29.97	100	29.94	100	29.96	100		
						31.84	65
						34.50	43
						36.32	100
						47.62	26
52.62	25	52.55	22	52.50	19		
						56.62	42

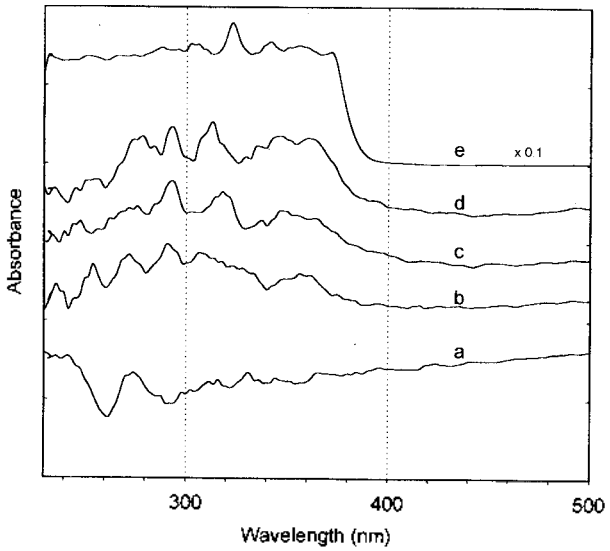

Figure 2. UV-VIS DRS (scan speed: 600 nm/min) of (a) H-Y, Zeolite H-Y after the exposure to Zn vapor for (b) 6 h (c) 9 h (d) 12 h followed by oxidation in the air at 450 °C, and (e) bulk ZnO powder.

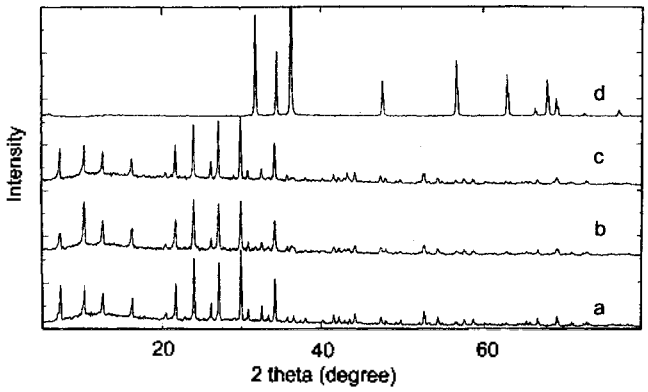

Figrue 3. XRD spectra of (a) Na-A, Zeolite Na-A after the exposure to Zn vapor for (b) 3 h (c) 12 h followed by oxidation in the air at 450 °C, and (d) bulk ZnO powder.

is believed that a decrease in the size of semiconductor results in an increase of band gap energy.[4,13] We believe that the overall pattern of peaks among various samples suggests the transition of the molecular electronic levels due to the change of configurations from bulk ZnO, although we are not able to correlate the pattern of peaks and the configuration of ZnO at current stage.

XRD spectra of zeolite Na-A, after Zn vapor deposition and oxidation, is compared with the XRD spectrum of zeolite Na-A in Figure 3. They all show the unique peaks of zeolite A. The peak positoins are slightly different and the relative peak intensities change with the exposure time to Zn vapor, which may imply the ZnO confinement. However, the XRD peaks corresponding to ZnO do not appear in the samples as shown in Figure 3-b, -c, -d. The UV-VIS DRS in Figure 4 show similar characteristics as those of ZnO/H-Y. Several peaks in the range of 280-330 nm, and the growing peaks in the range of 330-390 nm with the longer exposure time to Zn vapor, are the same as those of ZnO/H-Y. However, the rate of peak height

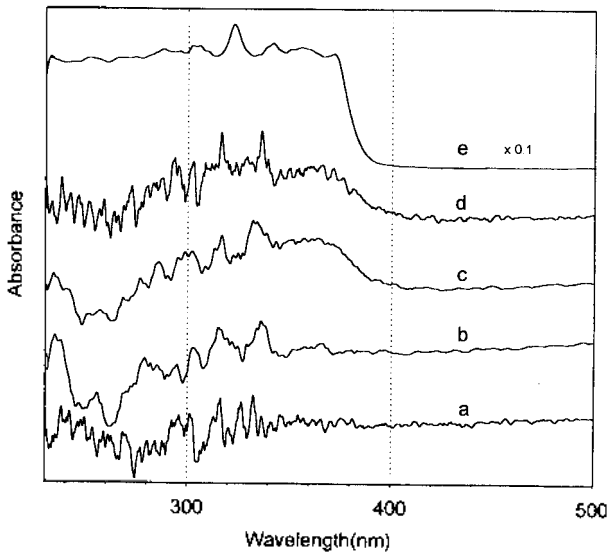

Figure 4. UV-VIS DRS (scan speed: 300 nm/min) of (a) Na-A, Zeolite Na-A after the exposure to Zn vapor for (b) 3 h (c) 9 h (d) 12 h followed by oxidation in the air at 450 °C, and (d) bulk ZnO powder.

Table 3. Comparison of mole ratio Zn/Al for samples of H-Y and Na-A after the exposure to Zn vapor followed by oxidation in the air at 450 °C

Exposure time		12	9	6	3	0
Zn/Al	H-Y	11.15	0.79	0.22	-	0.00
	Na-A	0.14	0.10	-	0.06	0.00

growing is more rapid for ZnO/H-Y compared to ZnO/Z-A in the range of 330-400 nm. This means that the formation of ZnO is more feasible and the size of ZnO cluster is likely to be larger in the cages of H-Y than in those of Z-A as expected from the bigger cage size in H-Y. Even though XRD spectra do not reveal peaks of ZnO explicitely, it implicate the incorporation of ZnO clusters by the changes of relative peak intensities. ZnO peaks may not be observed in XRD due to the small size or less uniformity.

Mole ratios from ICP results confirm that the Zn loading level increases by increasing the exposure time of zeolite to Zn vapor in both systems as shown in Table 3. The amount of Zn is greater in zeolite H-Y than in Z-A. This is consistent with the result of UV-VIS DRS, which indicate that ZnO formation is more feasible and that the ZnO nano-cluster is larger in the cages of H-Y than in those of Z-A.

Finally, let's examine where the ZnO clusters may be formed in zeolite. In the case of fully Zn exchanged zeolite Y, Zn is coordinated to oxygen atoms in 6-ring window which forms sodalite cage.[9] The longer the reaction time of zeolite with Zn vapor is, the higher the loading level of Zn is expected. If Zn vapor is under redox reaction when the zeolites are exposed to, it is suggested that the ZnO is formed within the sodalite cage, where Zn^{2+} ion sits near the center of 6-ring window of sodalite cage. However, the charge and location of Zn in the zeolites after the Zn vapor deposition is not clear. The more pronounced change of peaks in 330-390 nm in UV-VIS DRS and higher Zn loading from ICP results for ZnO/H-Y compared to ZnO/Z-

A hint the possibility of ZnO formation in the alpha cage. Since the size and number of beta cage are same in both zeolite Y and A, they would lead to the same size of ZnO cluster. Then it is difficult to explain the above experimental observation without guessing the ZnO formation in the alpha cage. Therefore, we expect some Zn vapor absorption, which would lead to ZnO formation in the alpha cage of zeolites.

Further studies are in progress to confirm the existence of nano clusters in zeolite and to investigate the nature of the cluster. We are also studying the size and configuration of ZnO nano clusters in zeolites by theoretical approach. We will continue to investigate the electronic properties of ZnO nano interfaces, once we secure the uniform ZnO cluster distribution in zeolite pores.

Acknowlegement. This work was supported by Korean Science and Engineering Foundation (961-0305-051-2). HML wishes to acknowledge the financial support of the Korea Research Foundation made in the program year 1997.

References

1. Srdanov, V. I.; Blake, N. P.; Markgraber, D.; Metiu, H.; Stucky, G. D.; *Advanced Zeolite Science and Applications: Studies in Surface Science and Catalysis*; Janson, J. C.; Stöcker, M.; Karge, H. G.; Weitkamp, J. Eds.; Elsevier: Amsterdam, 1994; Vol. 85, p. 115.
2. Kang, Y. C.; Park, S. B.; *J. Mat. Sci. Lett.* **1997**, *16*, 131.
3. Herron, N.; *J. Incl. Phen. Mol. Recog. Chem.* **1995**, *21*, 283.
4. Herron, N.; Wang, Y.; Eddy, M. M.; Stucky, G. D.; Cox, D. E.; Moller, K.; Bein, T.; *J. Am. Chem. Soc.* **1989**, *111*, 530.
5. Moller, K.; Eddy, M. M.; Stucky, G. D.; Herron, N.; Bein, T.; *J. Am. Chem. Soc.* **1989**, *111*, 2564.
6. Liu, X.; Thomas, J. K.; *Langmuir*, **1989**, *5*, 58 (1989).
7. Bartkowiak, M.; Mahan, G. D.; Modine, F. A.; Alim, M. A.; *J. Appl. Phys.* **1996**, *79* (1), 273.
8. Türk, T.; Sabin, F.; Vogler, A.; *Mater. Res. Bull.* **1992**, *27*, 1003.
9. Peapples-Montgomery, P. B.; Seff, K.; *J. Phys. Chem.* **1992**, *96*, 5962.
10. *Inorganic Synthesis*; Holt, S. L. Ed.; John Wiley & Sons: New York, 1983; Vol. 22, Chapter 1.
11. *Collection of Simulated XRD Powder Patterns For Zeolites (3rd ed.)*; Treacy, M. M. J.; Higgins, J. B.; von Ballmoos, R. Eds.; Elsevier Science Inc.: New York, 1996.
12. Szostak, R.; *Molecular Sieves: Principles of Synthesis and Identification*; Van Nostrand Reinhold, New York, 1989; Chapter 5.
13. Wark, M.; Kessler, H; Shultz-Ekloff, G.; *Microporous Mater.* **1997**, *8*, 241.

Synthesis of Copper(II) Complexes of Pentaamine Ligands Containing One 1,3-Diazacyclohexane Ring

Shin-Geol Kang*, Kiseok Ryu, and Jinkwon Kim†

Department of Chemistry, Taegu University, Kyungsan 712-714, Korea
†Department of Chemistry, Kongju National University, Kongju 314-701, Korea
Received March 13, 1998

Various types of polyaza macrocyclic copper(II) and nickel (II) complexes containing N-CH_2-N linkages have been prepared by one-pot metal template condensation of amines and formaldehyde (for example, *see Eq.* (1)[6,7]).[1-13] However, examples of non-macrocyclic polyamine complexes containing N-CH_2-N linkages are relatively rare.[12-14] Recently, the copper(II) complex of the non-macrocyclic pentaamine ligand **1** containing one 1,3-diazacyclohexane ring was prepared in our group by the reaction of *Eq.* (2).[12] The complex $[Cu(\mathbf{1})]^{2+}$ has a square-planar coordination geometry with a 5-6-5 chelate ring sequence, likewise the tetraamine complex $[Cu(\mathbf{6})]^{2+}$. However, chemical properties of $[Cu(\mathbf{1})]^{2+}$ such as kinetic behaviors in acidic solutions are different from those of the copper(II) complexes of **6** and other related tetraamine ligands.[12] Therefore, we have been interested in the synthesis of various types of such non-macrocyclic complexes to further investigate the effects of the structural characteristics on their properties.

In this work we prepared new copper(II) complexes of **2-4** from the reactions of *Eqs.* (2) and (3). The crystal structure of $[Cu(\mathbf{3})](ClO_4)_2$ was also determined to investigate the coordination behaviors of the hydroxyethyl group. To our knowledge, $[Cu(\mathbf{4})]^{2+}$ is a rarely prepared polyamine complex in which four nitrogen atoms are coordinated with a 5-6-6 chelate ring sequence. Although various polyamine complexes with a symmetrical 5-6-5 or 6-5-6 chelate ring sequence have been prepared, those with an asymmetrical 5-6-6 chelate ring sequence have not been widely investigated because of synthetic difficulties.[15]

$$M^{2+} + 2H_2N(CH_2)_2NH(CH_2)_3NH_2 + 4HCHO \longrightarrow [M(\mathbf{5})]^{2+} \quad (1)$$
(M = Ni or Cu)

$$Cu^{2+} + H_2N(CH_2)_2NH(CH_2)_3NH_2 + H_2N(CH_2)_2NHR + 2HCHO \longrightarrow [Cu(L)]^{2+} \quad (2)$$
R = H for **1** (L = **1**, **2**, or **3**)
R = C_2H_5 for **2**
R = $(CH_2)_2OH$ for **3**